



Design of friction connections in R.C. structures with hybrid steel-trussed-concrete beams

Piero Colajanni^a, Lidia La Mendola^a, Alessia Monaco^b, Salvatore Pagnotta^a

^a Department of Engineering, University of Palermo, Viale delle Scienze, Edificio 8 - 90128 Palermo, Italy

^b Department of Architecture and Design, Politecnico di Torino, Viale Mattioli 39 - 10125 Torino, Italy

Keywords: friction dampers; hybrid steel-trussed-concrete beams; cyclic behaviour of joints; finite element models

ABSTRACT

In this work a feasibility study on the use of friction devices within beam-to-column joints of RC structures is conducted. The connection is made between RC columns cast in-situ and semi-prefabricated steel-concrete beams, named Hybrid Steel-Trussed-Concrete Beams (HSTCBs). Nowadays, HSTCBs are widely adopted in civil and industrial buildings and, therefore, it is required to evaluate their compliance with the capacity design criteria and their seismic energy dissipation capability. However, the design of the reinforcement of such beams usually lead to the adoption of large amount of steel within the panel zone which becomes potentially vulnerable to the effects of seismic cyclic actions and dramatically reduce the dissipation capacity of the entire structure. Therefore, the introduction of friction dampers in the HSTCB-to-column joints is investigated in order to evaluate the ability of the device in preventing the main structural elements from damage and limiting the cracking of the panel zone, thanks to the increase of the bending moment lever arm, which reduces the shear forces in the joint. The feasibility study is firstly conducted through the development of design criteria for the pre-dimensioning of the device and, successively, the proposed solution is validated through the generation of finite element models.

1 INTRODUCTION

The most recent design strategies of multi-storey framed structures are increasingly welcoming the adoption of innovative techniques for the seismic energy mitigation, in order to guarantee a highly dissipative global behaviour able to prevent the structure from collapse with consequent loss of human lives. In particular, there is a large interest in the study of those devices able to absorb the whole seismic energy avoiding the damage of the primary load-bearing structural elements. Thus, irreversibly damage after a violent seismic event, resulting in extremely high economic costs for their structural repair is avoided. (Borzouie et al. 2016; Chanchi Golondrino et al. 2018, Chanchi Golondrino et al. 2018; Francavilla et al. 2016; Khoo et al. 2015; Latour and Rizzano 2015; Mitsui et al. 2018; Tartaglia et al. 2019; Tartaglia et al. 2018; Ukanwa et al. 2018; Volynkin et al. 2019; Zimbru et al. 2018a; Zimbru et al. 2018b). In the last thirty years, Hybrid Steel-Trussed-Concrete Beams (HSTCBs) have been widely used in civil and

industrial buildings and, therefore, their mechanical performance must be evaluated for ensuring the compliance with the capacity design criteria and achieving the adequate amount of seismic energy dissipation, particularly in the beam-to-column joints (Colajanni et al. 2016; Colajanni et al. 2015a; Colajanni et al. 2017; Colajanni et al. 2018a; Colajanni et al. 2015b; Monaco 2016). However, HSTCBs are often designed to exploit the steel reinforcement made up of a steel truss in order to cover large spans with reduced depth. In such cases, a large amount of steel reinforcement is required within the panel zone which is often made using large diameter rebar. These features make both the end of the beam and the joint potentially vulnerable to the effects of cyclic actions induced by the earthquake and dramatically reduce the dissipation capacity of the entire structure (Colajanni et al. 2015b; Colajanni et al. 2018b).

For this purpose, the present work investigates the introduction of friction dampers in the HSTCB-to-column joints of framed structures in seismic areas, adequately designed for their application on RC frames. The use of friction devices prevents the main structural elements from

damage and limits the cracking of the panel zone thanks to the increase of the bending moment lever arm and the entity of the bond actions transmitted by the beam rebars, which reduces the shear forces in the joint (Colajanni et al. 2016, 2015a; D'Aniello et al. 2017; Faella et al. 1998; Francavilla et al. 2018; Lemos et al. 2018; Tartaglia et al. 2017).

The feasibility study is firstly conducted through the development of design criteria for the pre-dimensioning of the device and, successively, the proposed solution is validated through the generation of finite element models.

2 DESIGN CRITERIA

The dissipative connection system between R.C. column and HSTCB represented in Figure 1 is constituted by the following components: - the upper T-stub connection anchored to the column and bolted to a "C" steel profile which is welded to the upper longitudinal rebars of the steel truss of the HSTCB; - the friction connection on the bottom, constituted by a vertical central steel plate with curved slotted holes and steel angles anchored to the column; the latter realize the friction connection with the central slotted plate and eventual plies of friction material. These elements are connected by high strength friction bolts properly preloaded according to the slip force required.

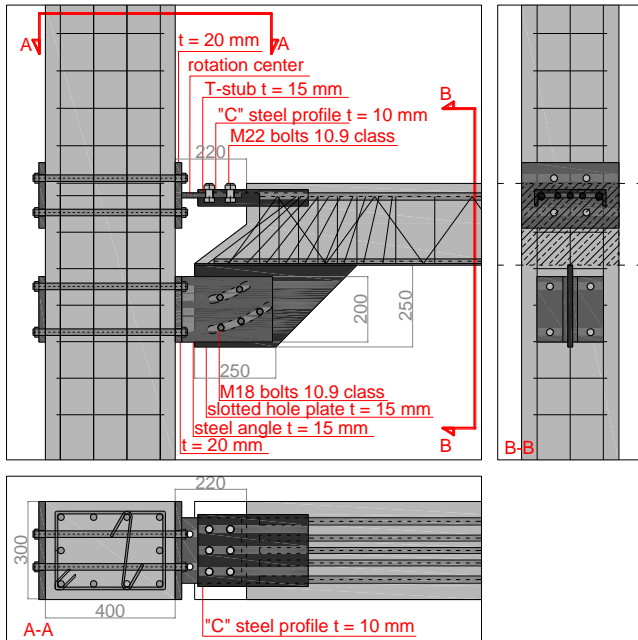


Figure 1. Structural solution adopted for the connection.

2.1 Calculation of the design parameters

The design of the friction connection requires the definition of the design bending moment M_d

which corresponds to the slippage of the device. Such a solicitation should be calculated from the structural analysis of the frame in which the friction connection needs to be used. The main scope is avoiding the slip of the device within the service limit state and allowing the dissipation under seismic events.

In this paper, a theoretical feasibility study is conducted and the specific structural details of the construction are not taken into account. Therefore, a design value of the bending moment is arbitrarily assumed $M_d=110$ kNm. Moreover, with the aim of providing overstrength to all components of the friction connection with respect to the load able to activate the slippage, an overstrength coefficient Ω_μ is adopted. In the absence of experimental campaigns for the assessment of the characteristic values of the static and dynamic friction coefficient, in this study the value $\Omega_\mu = 1.5$ is assumed. Therefore, the overstrengthened design bending moment is equal to $M_{Rd} = \Omega_\mu M_d = 1.5 \times 110 = 165$ kNm and, assuming a length L of 5m for the beam, the shear resistance results $V_{Rd} = 2M_{Rd}/L = 66$ kN in the absence of distributed loads.

The friction damper is designed to withstand a tensile slip force F_d equal to the design bending moment M_d divided by the lever arm z which is equal to 380 mm in our conception of the geometry of the device, which will be described more in detail later

$$F_d = \frac{M_d}{z} = \frac{110}{0.38} = 289.5 \text{ kN} \quad (1)$$

It is assumed to use five M18 bolts 10.9 class, whose area is $A_{res}=192$ mm² and yielding and ultimate strength are $f_{yb}=900$ MPa and $f_{ub}=1000$ MPa. Therefore, the preloading force F_{pc} of each bolt is equal to:

$$F_{pc} = 0.7 f_{ub} A_{res} = 134.4 \text{ kN} \quad (2)$$

According to Eurocode 3 (CEN 2005a,b), the sliding force $F_{s,Rd}$ is calculated through the following expression:

$$F_{s,Rd} = \frac{k_s n_b n_s \mu}{\gamma_{M3}} F_{pc} \quad (3)$$

where:

- k_s is a coefficient that depends on the shape of the slotted hole (in the current case it is equal to 0.63);
- n_b is the number of bolts (5 in this case);
- n_s is the number of surfaces in contact (2 in this case);

- μ is the friction coefficient (herein assumed equal to 0.4);
- γ_{M3} is a safety factor equal to 1.25.

Equation (3) provided in the Code, is aimed at the design of connections in which the sliding is prevented until the ultimate limit state and therefore the coefficients k_s and γ_{M3} are used. Conversely, in the design of the connection herein presented, such coefficients are not taken into account.

Furthermore, concerning the preloading force, several studies in the literature show that the value of F_{pc} decreases progressively due to creep phenomena which is affected to high amount of preloading force applied to the bolt. With the aim of limiting these effects, in Ferrante Cavallaro et al. (2017, 2018) to contain the preloading force in the bolts within the range 30-60% of the maximum load suggested by the Code is proposed. Therefore, in the present study, the design sliding force $F_{s,d}$ is:

$$F_{s,d} = t_s n_b n_s \mu F_{pc} \quad (4)$$

where the parameter t_s is introduced for representing the stress level of the bolt, i.e. the aliquot of the maximum preload that is applied to the bolt and which is set between 0.3 and 0.6 as mentioned before. In particular, by equating Eq. (1) and Eq. (4) a stress level $t_s=0.538$ is obtained. Successively, the design preloading force $F_{pc,d}$ to be applied to each bolt is:

$$F_{pc,d} = t_s F_{pc} = 0.538 \cdot 134.4 = 72.3 \text{ kN} \quad (5)$$

Based on these calculations and on the geometrical requirements provided in Eurocode 3 (CEN 2005a,b), the conception of the damping device is depicted in Figure 2. Five bolts collocated on two rows are used and curved slotted holes are designed, with rotation center C indicated in the same figure. The main dimensions indicated are equal to: $L_1 = 158 \text{ mm}$; $L_2 = 342 \text{ mm}$; $L_3 = 5 \text{ m}$; $\alpha = 68^\circ$ and $\beta = 22^\circ$.

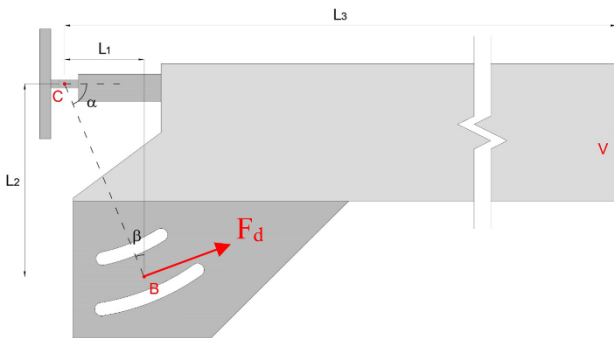


Figure 2. Geometric scheme of the friction device.

It could be worth to observe that the design is conceived so that the diameter of the preloaded bolts can be easily changed providing the same preloading force given in Eq. (5) using a different stress level t_s . In this way it is possible to adopt HV bolt assemblies using the most common bolt diameters available in the market, for instance M16 or M20 bolts.

2.2 Dimensioning of the connections

The device is connected to the beam and the column through bolted steel plates, T-stub and angles which are depicted in Figures 3 and 4. In particular, Figure 3 shows the T-stub designed for the upper connection. The dimensions are the following: $b_{fl} = 300 \text{ mm}$, $h_{fl} = 200 \text{ mm}$, $t_{fl} = 20 \text{ mm}$, $t_w = 15 \text{ mm}$, $b_w = 200 \text{ mm}$, $l_w = 185 \text{ mm}$.

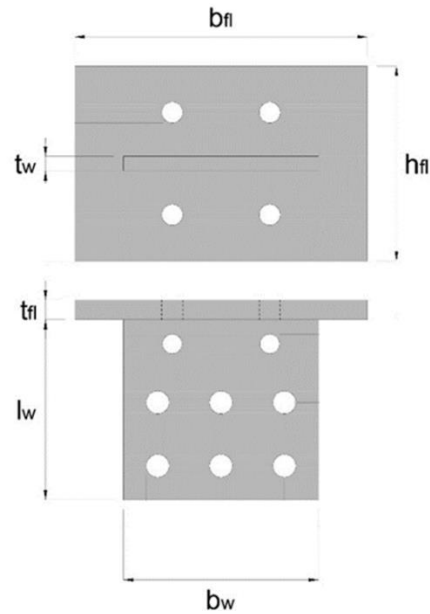


Figure 3. Dimensions of the T-stub.

The connection between T-stub and beam is designed as a classical friction bolted connection where the design sliding force $F_{d,h}$ is evaluated as the horizontal component of the force defined in Eq. (1), i.e.:

$$F_{d,h} = \Omega_\mu F_d \sin(\alpha) = 402.6 \text{ kN} \quad (6)$$

α being the angle between the beam longitudinal axis and the axis connecting the rotation center C and the application point of the sliding force B indicated in Figure 2. For this connection, six M22 bolts of 10.9 class are used. The number of bolts required has been calculated through the following equation:

$$n_b = \frac{F_{d,h} \gamma_{M3}}{k_s n_s \mu F_{pc}} = \frac{402.6 \cdot 1.25}{1 \cdot 1 \cdot 0.4 \cdot 212.1} = 5.93 \Rightarrow 6 \quad (7)$$

The thickness of the T-stub web is dimensioned assuming that it must absorb only the traction

expressed by Eq. (6) while the capacity to withstand the shear force is completely demanded to the steel angles of the lower connection depicted in Figure 4.

The two lower steel angles are bolted to the slotted hole central plate. The dimensions of the angles are: $h = 200$ mm, $b_{fl} = 80$ mm, $t_{fl} = 20$ mm, $t_w = 15$ mm, $l_w = 280$ mm, $d_w = 19.5$ mm, $p_1 = 65$ mm, $p_2 = 90$ mm, $e_1 = 48$ mm.

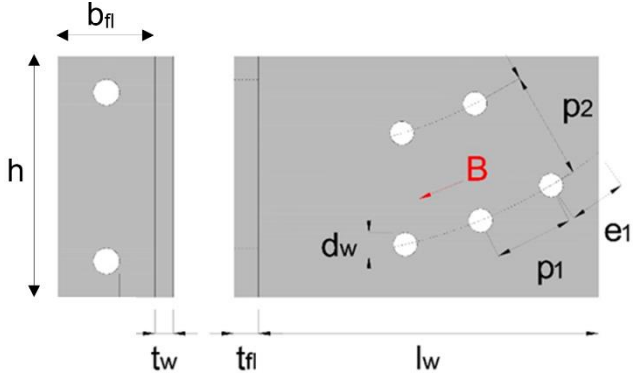


Figure 4. Dimensions of the steel angle.

In the figure, the point B represents the centroid of the preloading forces of the five bolts.

Each angle is subjected to one half of the force expressed by Eq. (1) according to the horizontal and vertical components (B_o and B_v respectively) which can be calculated through the following expressions:

$$B_o = \frac{1}{2} \Omega_\mu F_d \sin(\alpha) = 201.3 \text{ kN} \quad (8)$$

$$B_v = \frac{1}{2} \Omega_\mu F_d \cos(\alpha) = 81.4 \text{ kN} \quad (9)$$

Therefore, the web of the steel angle is dimensioned considering the bending moment in the presence of axial force while the flange is checked according to the plastic failure mechanisms of Eurocode 3 (CEN 2005a,b).

3 FINITE ELEMENT MODEL

The feasibility study is conducted by means of the Finite Element Method (FEM) for the simulation of the structural behaviour of the dissipative connection. In this paper a first modelling approach is described, in which the structural details of the column have been neglected as well as the connection to the pillar: the column is assumed to behave according to an unlimited elastic behaviour and the efficacy of the anchors is supposed to be perfect.

Preliminary FEM analyses showed that the system exhibited no sufficient stiffness in the in-plane direction in the absence of inclined rebars

welded on the lower plate of the HSTCB. These 12 mm diameter stirrups are depicted in Figure 5; they have variable inclination and allow the activation of the stress transfer mechanism between concrete, steel top chord and slotted-hole central plate.

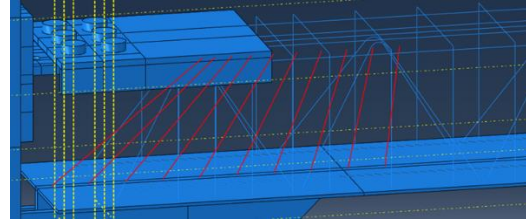


Figure 5. Structural solution adopted for the simulation.

The main features of the model are reported in Figure 6. The response of the beam-to-column connection is reproduced assuming for the column a cross-section of 300x400 mm and a length of 3 m. The column has pinned supports and a cyclic displacement of ± 100 mm is applied to the beam tip. Before the application of the displacement history, the preloading force is applied to the bolts of the damping device. The finite elements used are represented in Figure 7. In particular, first order tetrahedral are used for all components with the exception of column and C steel profile for which linear bricks are selected. The model is basically focused on the simulation of contacts. In particular, the friction formulation is adopted imposing the value of the friction coefficient between two adjacent surfaces in the damping device. Conversely, friction is assumed negligible between the bottom steel plate and the concrete of the HSTCB as well as between the concrete and the “C” profile partially embedded within the beam for ensuring the upper connection. Finally, perfect bond is assumed for the contact between concrete and diagonal, longitudinal and transversal reinforcement of the HSTCB (Figure 8).

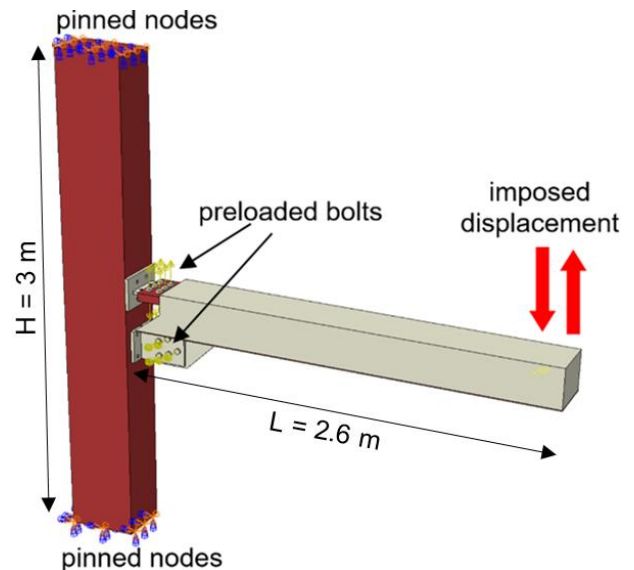


Figure 6. Boundary and loading conditions.

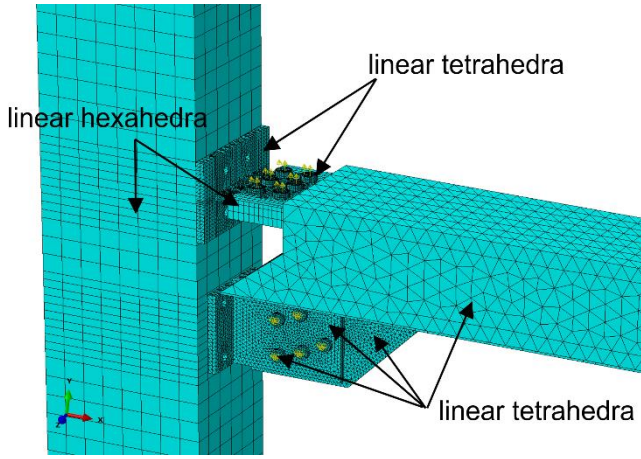


Figure 7. Mesh of the elements.

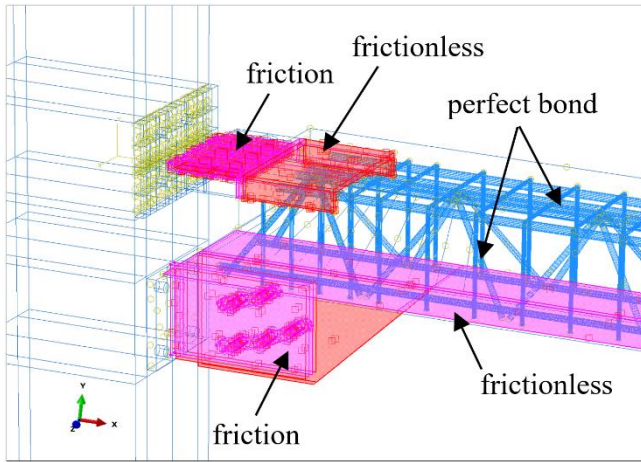


Figure 8. Surfaces for the definition of contacts.

As regards materials, the steel elements are modelled using an elasto-plastic behaviour whose main features are reported in Table 1. In particular the table reports the elastic modulus (E_s), the yield stress (f_y) and the ultimate strain (ϵ_u) for each component of the friction device. For the concrete material, a compressive strength of 25 MPa and an elastic modulus of 28960 MPa have been adopted. The plastic behaviour of concrete is modelled using the Concrete Damaged Plasticity model based on the theory of plastic continuous damage of quasi-brittle materials. The overall stress-strain curve reported in Figure 9 has been implemented.

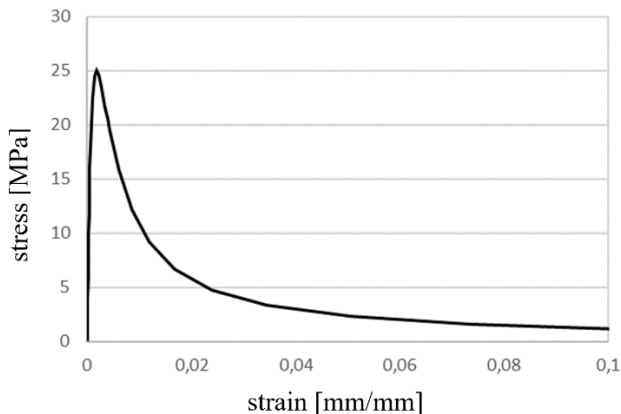


Figure 9. Compressive stress-strain law of concrete.

Table 1. Mechanical features of the steel of the device.

	E_s [GPa]	f_y [MPa]	ϵ_u [%]
plates	210	355	0.3
bolts	210	900	0.3

4 RESULTS

The results are presented in terms of load-displacement curves and stress contours for both monotonic and cyclic response.

Figure 10 reports the monotonic load-displacement plot. It can be observed that the system is able to provide the expected response. In particular, three phases can be individuated:

- Phase 1: the friction device does not slip; the behaviour of the system is almost elastic without relevant changes in stiffness;
- Phase 2: the sliding is activated and the behaviour of the system turns into plastic type, exhibiting a slight hardening probably due to the plasticization of the upper connection. The deformations of the beam slightly move the rotation center assumed during the design;
- Phase 3: the design displacement limit is reached; a progressive increment in load is caused by the contact between the bolt shank and the slotted hole internal surfaces.

Figure 11 reports the stress state in the device during the analysis between phase 1 and 2. The figure shows that all steel components of the device are in the elastic range of their constitutive behaviour.

Similarly, the stress state in the concrete block is represented in Figure 12. In particular, the minimum principal stresses are represented. The compression levels achieved are satisfactory in the whole concrete volume with the exception of the stress localization within the circled area in the figure, where the bottom steel plate of the HSTCB is not effective in transferring the internal forces coming from the slotted hole plate.

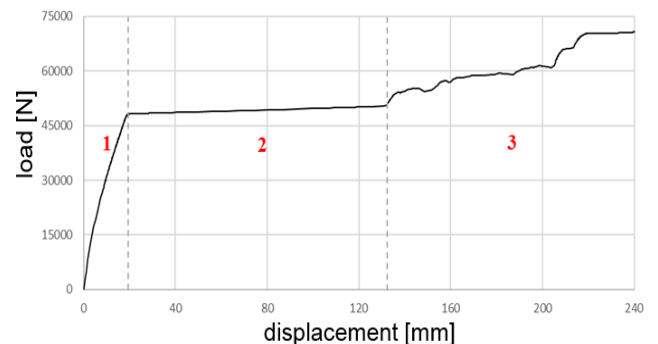


Figure 10. Monotonic load-displacement curve.

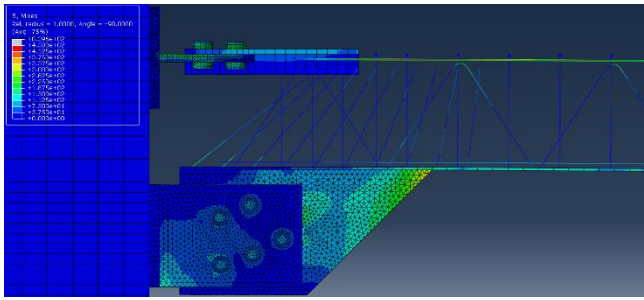


Figure 11. Stress state in the device between phase 1 and 2.

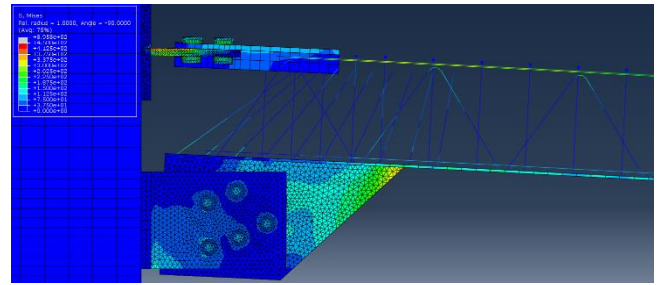


Figure 14. Stress state in the device between phase 2 and 3.

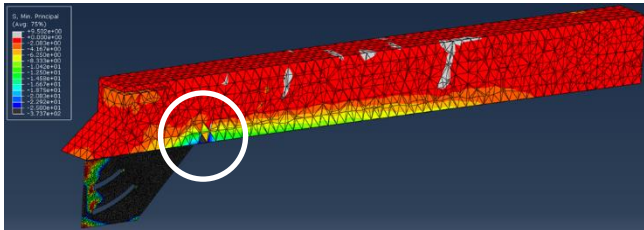


Figure 12. Minimum principal stresses in the concrete between phase 1 and 2.

In Figure 13 the plastic maximum principal strains in the concrete are depicted. Three different cracked areas can be individuated:

- outer boundaries of the beam, i.e. beam extrados (1): here the concrete cracking is due to the flexural tensile stresses;
- concrete cover of the C steel profile (2): the deformations of the steel profile induce the damage of the concrete cover;
- bottom plate-concrete interface (3): the bottom steel plate and the concrete surfaces in contact experience damage because of the significant tensile stresses due to the inclined stirrups.

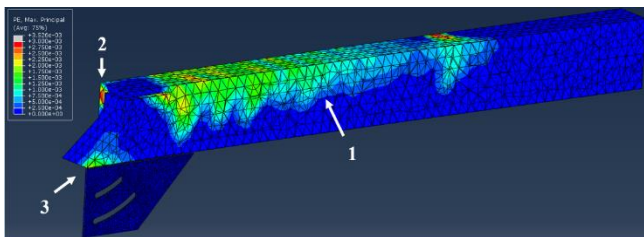


Figure 13. Maximum principal strains in the concrete between phase 1 and 2.

Similarly, it is possible to analyse the numerical output in the transition between phase 2 and 3 previously reported in Figure 10. In particular, Figure 14 shows the stress state in the steel device which can be compared with Figure 11. The stress level in the steel elements is almost unchanged; the most relevant difference can be viewed in the behaviour of the T-stub connected to the “C” profile: here the increase of the rotation of the system produces the increase in the flexure to which the T-stub is subjected.

In the same way, the principal stresses in the concrete shown in Figure 15 prove to keep almost unchanged.

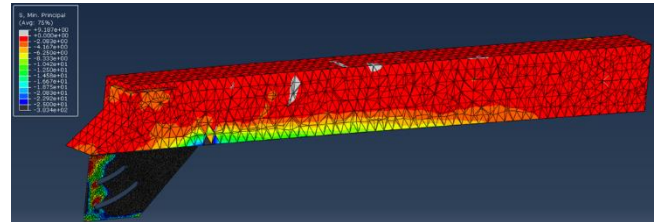


Figure 15. Minimum principal stresses in the concrete between phase 2 and 3.

Finally, Figure 16 shows the cracked concrete in the transition between phase 2 and 3. In particular, the maximum principal strain contour indicates that there is a slight increment of the crack propagation especially in the area next to the C steel profile embedded within the concrete. This phenomenon might be due to the significant increment of the flexure of the “C” profile, despite its high stiffness. Such a flexure induces a progressive degradation of the concrete cover around the steel profile.

The output of Phase 3 is not analysed because it refers to the behaviour of the device beyond the design working condition.

The cyclic response is reported in Figure 17. From the load-displacement curve reported in the figure, it can be observed that the system behaves according to the design requirements, i.e. it exhibits a symmetric response for hogging and sagging bending moment and does not evidence any damage in the loading-unloading phases. The analysis of the stress state is the same already described for the monotonic numerical test.

Conversely, the attention is focused on the plasticization cumulated on the device components at the end of the cyclic test. In particular, Figure 18 reports the distribution of the equivalent plastic strains: it can be observed that all steel elements are in the elastic range with the exception of the horizontal flange of the T-stub which behaves in the plastic range according to the design requirements.

As regards the concrete block, it can be noteworthy to assess the cracking state of the material on the basis of the equivalent tensile plastic strains represented in Figure 19. As expected, in the inner rim of the beam, at its intrados, the concrete cracks when the beam is

subjected to positive bending moment. In the same time, the cyclic action produces a greater deformation of the C steel profile of the upper connection with respect to the behaviour observed in the monotonic simulation, increasing the plastic strains of the surrounding concrete cover.

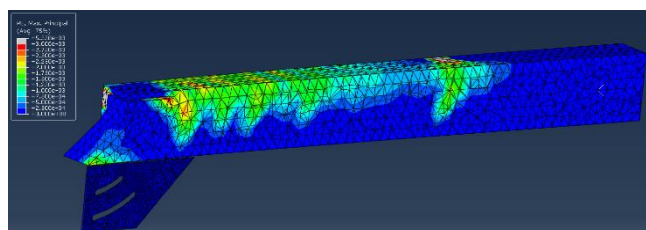


Figure 16. Maximum principal strains in the concrete between phase 2 and 3.

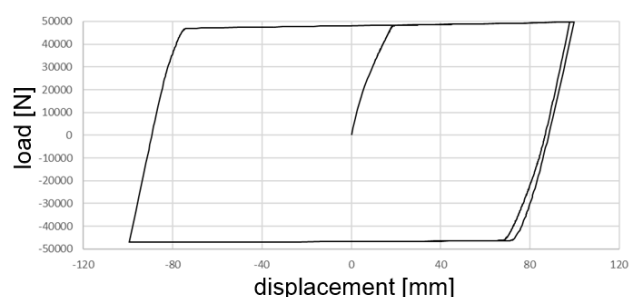


Figure 17. Cyclic load-displacement curve.

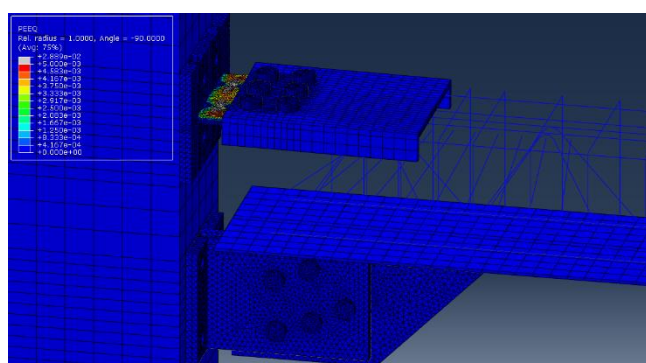


Figure 18. Plastic strain distributions at the end of the cyclic FE test.

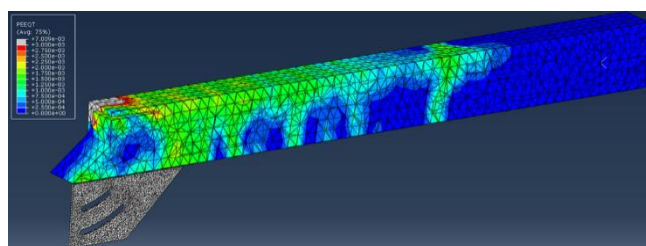


Figure 19. Maximum principal strains in the concrete at the end of the cyclic FE test.

5 CONCLUSIONS

In this study the introduction of friction dampers in the HSTCB-to-column joints of framed structures has been investigated. The calculation has been conducted according to the current prescriptions for buildings in seismic areas and the

damping device has been adequately designed for its application on R.C. frames. The friction device components and the connections to beam and column have been dimensioned and verified according to Eurocode 3 prescriptions. Conversely, the structural details of the column and the connection within the latter have been neglected, in the meaning that the column behaviour has been assumed linear elastic and the efficacy of the anchors perfect.

The device has been conceived for a working level of the preloaded bolts of 0.54 adopting an overstrength coefficient of 1.5.

The feasibility study has been firstly conducted through the development of design criteria for the pre-dimensioning of the device and, successively, the proposed solution has been validated through the generation of finite element models.

Monotonic and cyclic tests have been simulated, showing that the device behaves according to the design requirements. In particular, the steel elements remain elastic with the exception of the T-stub components in which the rotation center of the system was theoretically assumed during the design process. The cyclic behaviour has shown a symmetric response under hogging and sagging bending moment without degradation during the unloading and reloading phases.

ACKNOWLEDGEMENTS

The economic support to the research of the SICILFERRO TORRENOVESE s.r.l. company is acknowledged, and the Authors thank Dr. Mauro Scurria and Eng. Nicolò Cancelliere for helpful discussion and active participation in the research project.

REFERENCES

- Borzouie, J., G. A. Macrae, J. G. Chase, G. W. Rodgers, and G. C. Clifton. 2016. Experimental Studies on Cyclic Performance of Column Base Strong Axis-Aligned Asymmetric Friction Connections. *Journal of Structural Engineering (United States)*, **142**(1).
- CEN EN 1993-1-1-Eurocode 3: Design of Steel Structures. Part 1: General Rules and Rules for Buildings. Comité Européen de Normalisation, 2005a.
- CEN EN 1993-1-8-Eurocode 3: Design of steel structures – Part 1-8: Design of joints, 2005b.
- Chanchi Golondrino, J. C., G. A. MacRae, J. G. Chase, G. W. Rodgers, and G. C. Clifton. 2018. Hysteretic Behaviour of Asymmetrical Friction Connections Using Brake Pads of D3923. *Structures*, **16**, 164–75.
- Chanchi Golondrino, J. C., G. A. MacRae, J. G. Chase, G. W. Rodgers, and G. C. Clifton. 2019. Asymmetric

- Friction Connection (AFC) Design for Seismic Energy Dissipation. *Journal of Constructional Steel Research*, **157**,70–81.
- Colajanni, P., L. La Mendola, M. Latour, A. Monaco, and G. Rizzano. 2015a. FEM Analysis of Push-out Test Response of Hybrid Steel Trussed Concrete Beams (HSTCBs). *Journal of Constructional Steel Research*, **111**, 88-102.
- Colajanni, P., L. La Mendola, M. Latour, A. Monaco, and G. Rizzano. 2017. Analytical Prediction of the Shear Connection Capacity in Composite Steel–concrete Trussed Beams. *Materials and Structures/Materiaux et Constructions*, **50**(1), art. no. 48.
- Colajanni, P., L. La Mendola, and A. Monaco. 2015b. Stiffness and Strength of Composite Truss Beam to R.C. Column Connection in MRFs. *Journal of Constructional Steel Research*, **113**, 86-100.
- Colajanni, P., L. La Mendola, and A. Monaco. 2018a. Review of Push-out and Shear Response of Hybrid Steel-Trussed Concrete Beams. *Buildings* **8**(10), art. n. 134.
- Colajanni, P., L. La Mendola, and A. Monaco. 2018b. Stress Transfer and Failure Mechanisms in Steel-Concrete Trussed Beams: Experimental Investigation on Slab-Thick and Full-Thick Beams. *Construction and Building Materials*, **161**(1), 267-281 .
- Colajanni, P., L. La Mendola, A. Monaco, and N. Spinella. 2016. Cyclic Behavior of Composite Truss Beam-to-RC Column Joints in MRFs. *Key Engineering Materials*, **711**, 681-689.
- D’Aniello, M., M. Zimbru, R. Landolfo, M. Latour, G. Rizzano, and V. Piluso. 2017. Finite Element Analyses on Free from Damage Seismic Resisting Beam-to-Column Joints. Pp. 802–14 in *COMPADYN 2017 - Proceedings of the 6th International Conference on Computational Methods in Structural Dynamics and Earthquake Engineering*. Vol. 1.
- Faella, C., V. Piluso, and G. Rizzano. 1998. Cyclic Behaviour of Bolted Joint Components. *Journal of Constructional Steel Research* **46**(1–3),433–34.
- Ferrante Cavallaro G, Francavilla A., Latour M., Piluso V., Rizzano G. (2017), “Experimental behaviour of innovative thermal spray coating materials for FREEDAM joints”. *Composites Part B*, 115, 289-299.
- Ferrante Cavallaro G., Latour M., Francavilla A., Piluso V., Rizzano G. 2018, “Standardised friction damper bolt assemblies time-related relaxation and installed tension variability”. *Journal of Constructional Steel Research*, 141, 145-155.
- Francavilla, A. B., M. Latour, V. Piluso, and G. Rizzano. 2016. Bolted T-Stub: A Refined Model for Flange and Bolt Fracture Modes. *Steel and Composite Structures* **20**(2), 267–93.
- Francavilla, A. B., M. Latour, V. Piluso, and G. Rizzano. 2018. Design of Full-Strength Full-Ductility Extended End-Plate Beam-to-Column Joints. *Journal of Constructional Steel Research*, **148**,77–96.
- Khoo, H. H., C. Clifton, G. Macrae, H. Zhou, and S. Ramhormozian. 2015. Proposed Design Models for the Asymmetric Friction Connection. *Earthquake Engineering and Structural Dynamics* **44**(8),1309–24.
- Latour, M. and G. Rizzano. 2015. Design of X-Shaped Double Split Tee Joints Accounting for Moment-Shear Interaction. *Journal of Constructional Steel Research* **104**,115–26.
- Lemos, A., L. S. da Silva, M. Latour, and G. Rizzano. 2018. Numerical Modelling of Innovative DST Steel Joint under Cyclic Loading. *Archives of Civil and Mechanical Engineering* **18**(3),687–701.
- Mitsui, K., M. Latour, G. Rizzano, A. Sato, and V. Piluso. 2018. Experimental and Numerical Analysis of the Ultimate Behaviour of Square Hollow Sections under Combined Axial and Bending Loads. *Ingegneria Sismica* **35**(2),5–22.
- Monaco, A. 2016. Numerical Prediction of the Shear Response of Semi-Prefabricated Steel-Concrete Trussed Beams. *Construction and Building Materials* **124**, 462-474
- Tartaglia, R., M. D’Aniello, and G. A. Rassati. 2019. Proposal of AISC-Compliant Seismic Design Criteria for Ductile Partially-Restrained End-Plate Bolted Joints. *Journal of Constructional Steel Research* **159**,364–83.
- Tartaglia, R., M. D’Aniello, G. A. Rassati, J. A. Swanson, and R. Landolfo. 2018. Full Strength Extended Stiffened End-Plate Joints: AISC vs Recent European Design Criteria. *Engineering Structures* **159**,155–71.
- Tartaglia, R., M. D’Aniello, G. A. Rassati, J. Swanson, and R. Landolfo. 2017. Influence of Composite Slab on the Nonlinear Response of Extended End-Plate Beam-to-Column Joints. *Key Engineering Materials* **763**,818–25.
- Ukanwa, K. U., C. G. Clifton, J. B. P. Lim, S. Hicks, and U. K. Sharma. 2018. Numerical Analysis of Plain and Steel Fiber Reinforced Concrete Filled Steel Tubular Slender Column. *Advanced Steel Construction* **14**(2),308–23.
- Volynkin, D., P. Dusicka, and G. C. Clifton. 2019. Intermediate Web Stiffener Spacing Evaluation for Shear Links. *Journal of Structural Engineering (United States)* **145**(2).
- Zimbru, M., M. D’Aniello, A. De Martino, M. Latour, G. Rizzano, and V. Piluso. 2018a. Investigation on Friction Features of Dissipative Lap Shear Connections by Means of Experimental and Numerical Tests. *Open Construction and Building Technology Journal* **12**,154–69.
- Zimbru, M., M. D’Aniello, A. Stratan, R. Landolfo, and D. Dubiná. 2018b. Finite Element Analysis of Composite Replaceable Short Links. *Key Engineering Materials* **763**,576–83.